Wide-Range Linear Iontronic Pressure Sensor with Two-Scale Random Microstructured Film for Underwater Detection

Shaowei Wu, Chengxiu Yang, Jiafei Hu,* Mengchun Pan, Weicheng Qiu, Yanrui Guo, Kun Sun, Yujing Xu, Peisen Li, Junping Peng, and Qi Zhang

Read Online

ACCESS | ![Metrics icon] Metrics & More | ![Recommendations icon] Article Recommendations | ![SI icon] Supporting Information

R²=0.9931
Slope=12.8
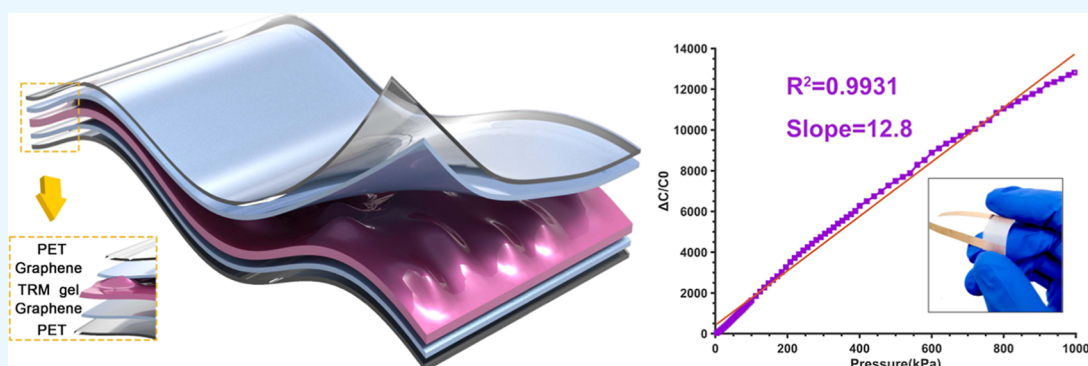
ABSTRACT: A broad linear range of ionic flexible sensors (IFSs) with high sensitivity is vital to guarantee accurate pressure acquisition and simplify back-end circuits. However, the issue that sensitivity gradually decreases as the applied pressure increases hinders the linearity over the whole working range and limits its wide-ranging application. Herein, we design a two-scale random microstructure ionic gel film with rich porosity and a rough surface. It increases the buffer space during compression, enabling the stress deformation to be more uniform, which makes sure that the sensitivity maintains steady as the pressure loading. In addition, we develop electrodes with multilayer graphene produced by a roll-to-roll process, utilizing its large interlayer spacing and ion-accessible surface area. It benefits the migration and diffusion of ions inside the electrolyte, which increases the unit area capacitance and sensitivity, respectively. The IFS shows ultra-high linearity and a linear range (correlation coefficient ∼ 0.9931) over 0−1 MPa, an excellent sensitivity (∼12.8 kPa⁻¹), a fast response and relaxation time (∼20 and ∼30 ms, respectively), a low detection limit (∼2.5 Pa), and outstanding mechanical stability. This work offers an available path to achieve wide-range linear response, which has potential applications for attaching to soft robots, followed with sensing slight disturbances induced by ships or submersibles.

1. INTRODUCTION

In the past few decades, flexible sensing technology has undergone rapid development, greatly expanding the power of natural sensors. On one hand, the noticeable progress of flexible electronic manufacturing technology on 3D freedom surfaces[1−3] and the great breakthrough of self-powered technology[4,5] greatly expand the application scenarios of flexible sensing. On the other hand, this substantial development is mainly reflected on sensitivity in the field of flexible pressure sensors.[6−8] The extremely high sensitivity of devices allows detecting weak changes in pressure, leading to many new applications such as human−computer interaction,[9−11] health monitoring,[12−14] and robotic tactile sensing.[15,16] Among them, ionic flexible sensors (IFSs) have produced a qualitative leap in sensitivity.[17,18] Similar to conventional parallel plate capacitors, the typical IFS consists of two electrodes with a dielectric layer sandwiched between them to transfer the pressure to a capacitive signal. However, due to the atomic scale distance (∼1 nm) between positive and negative charges

at the electrical double layer (EDL) interface, the capacitance of iontronic devices can be significantly increased, reaching about 6 orders of magnitude higher than that of parallel plate capacitors.[19]

The rational design of the material and microstructure of IFS dielectric layers ensures excellent sensitivity and linearity over a wide operating range. IFS typically utilizes ionic liquids (ILs)/ionic gels as active sensing elements to form ultra-high EDL capacitance. However, there are certain risks for ILs working in high-pressure situations resulting from the instability of the external packaging structure. In contrast,

ionic gel film constructed with surface microstructures is a more widespread choice in the sensitive electrolyte layer. It is easily prepared by cross-linking with excellent properties, such as high mechanical stability and a broad pressure sensitive window.[20] As one of the essential characteristics of IFS, sensitivity has recently been improved by various practical means. To this end, plenty of works have been devoted to optimizing the material system of ionic gels with the aim of increasing the mobile ions suspended in the matrix to maintain a high ionic conductivity.[21,22] Electrolyte membranes with unique surface patterns have been shown to be a practical approach to improving sensitivity and responsiveness.[23] Ionic gel films with microstructured surfaces are capable of outputting capacitance values under tiny strains, and these variable pattern designs emphasize increased sensitivity in a low-pressure region, including regularly raised arrays,[24,25] domed structures,[26] microcolumn arrays,[27] and surface patterns molded from randomly distributed microstructures (such as sandpaper and leaves).[28−30] As a typical representative, an ultra-sensitive capacitive pressure sensor based on a porous pyramidal dielectric layer exhibited the sensitivity of 44.5 kPa^{-1} in the pressure range of <100 Pa, which is unprecedented for the same type of pressure sensors.[24] However, the massive decrease in the sensitivity caused by the increasing applied pressure generates a clear inflection point in the entire response curve, which is not conducive to the design of back-end circuits. Meanwhile, this method requires a complicated process for fabricating molds. For another typical microstructure, Lu et al. prepared the gold electrodes into a soft micropillared structure contact surface. The response curve is divided into multiple interval segments (0−6, 6−12, and 12−176 kPa) with different sensitivities, which is because of the inconsistency of deformation in the columnar microstructure over the whole working range.[29] Nevertheless, the inverse features extracted from pillar template techniques are sophisticated, expensive, and extremely dependent on experimental operations. To solve this problem, Chhetry et al. fabricated a gel media layer with randomly distributed microstructures molded, releasing from sandpaper, and used a highly conductive porous percolation network prepared from polydimethylsiloxane reinforced silver nanowires (AgNWs/PDMS) as electrodes. It achieves high sensitivity, a low response time, a low limit of detection (LOD), and high stability in the low force range.[28] However, the sensitivity decreases sharply with increasing pressure, and the overall linearity in the operating range is still far from satisfactory.

It can be seen that although the sensitivity of the device has been substantially improved, it is difficult to maintain a consistent sensitivity in the overall operating range, resulting in the requirement for segmented calibration and the design of complex back-end decoupling circuits.[32] It is not conducive to the wide application of sensors. Furthermore, the high cost of manufacturing and the complicated process that requires manual handling significantly limit the performance consistency between different devices. It hinders the potential for large-scale industrial production and therefore the prospects for sensors. Therefore, it is necessary to develop a novel iontronic pressure sensor that maintains high linearity over the wide operating range.

In this study, we demonstrate an iontronic pressure sensor based on multilayer graphene electrode and ionic gel film with a two-scale random microstructure (TRM), which achieves a

good sensitivity (12.8 kPa^{-1}) and linearity (correlation coefficient R^2 = 0.9931) in a wide operating range (0−1 MPa) using multilayer graphene with a large specific surface area (SSA) and wide interlayer spacing as electrodes to form large EDL capacitance, thereby enhancing the sensitivity of the device. Based on poly (vinylidene fluoride-cohexafluoropropylene) (P(VDF-HFP)) and 1-ethyl-3-methylimidazolyl (trifluoromethylsulfonyl) imide ([EMIM][TFSI]), ionic gel was prepared as the precursor of TRM ionic film. Then the mixed dielectric solution is ultrasonically irradiated to form the exquisite first-scale microstructure, and the rougher second-scale microstructure is formed after casting on the sandpaper template. Thus, a particular type of solvent-free, independent solid polymer electrolyte film is developed as a high-capacitance dielectric material for the flexible pressure sensor. The two scales make TRM ionic gel film retractable and flexible active under external pressure. The simulation and experimental results show that in the absence of working interval segmentation, the obtained sensitivity remains consistent throughout the pressure interval and achieves a wide-range linear property. In addition, the sensor illustrates low dynamic response and relaxation times of about 20 and 30 ms, respectively, a low detection limit of 2.5 Pa, and a stability of more than 10,000 compression−release or 5000 bend−release cycles. As a demonstration, the IFS sensor can realize its application in underwater static pressure and propeller-induced wave disturbance detection. The overall results show that the method based on TRM ionic gel film and multilayer graphene electrodes provides a convenient way to develop a high-linearity sensor.

2. EXPERIMENTAL SECTION

2.1. Finite Element Simulation. Finite element analysis (FEA) of the force-induced deformation of sensor interface microstructure was performed using the commercial package Abaqus/Standard 2019. The electrode adopted the material parameters of polyethylene terephthalate (PET) in the software material library. The ionic gel was based on the classical hyperelastic material two-parameter Mooney−Rivlin model with σ_{01} = 0.78 and σ_{10} = 0.19. In order to simulate the differences between classical microstructure and TRM, the corresponding two-dimensional geometric models were established. The lower plate was set as a fixed constraint, and the normal direction displacement of the upper plate was specified. Through the static analysis of compression and release cycles, the kinetic energy of the system was guaranteed to be lower than the strain energy, and the calculation results were independent of time. The interface contact friction coefficient was set as 0.2, and the contact area between the output ionic gel and the upper electrode was output as a function of pressure.

2.2. TRM Iontronic Film Preparation. The ionic gel films used for the preparation of the iontronic sensor were fabricated based on a combination of two methods, namely, the premixed solution foaming treatment under ultrasonic irradiation and a gel injection molding on the basis of sandpaper templates. The ionic gel film was composed of a structuring polymer and an IL. In this study, all reagents were purchased from Sigma-Aldrich, China. Among them, P(VDF-HFP) (average MW ∼ 455,000, average M_n ∼ 110,000), [EMIM][TFSI] (HPLC ≥ 98%), and acetone (HPLC ≥ 99.5%) were employed as the structuring polymer, IL, and solvent, respectively. First, 12.5 wt % P(VDF-HFP) particles were added to acetone and stirred

until the particles dissolved to form a viscous liquid. Then [EMIM][TFSI] was added dropwise in P(VDF-HFP)–acetone solution at different concentration ratios and fully mixed. As a comparison, we divided this mixed solution in two-halves. We treated one part of it with ultrasonic irradiation at different frequencies and times, and the other part was treated without additional treatment as a control group, as shown in Supporting Information Table S1. After that, using #400 mesh silicon carbide sandpaper as a template, the composite was coated at 300 rpm for 60 s and placed in a fume hood for 24 h to remove the residual solvent. Finally, a microstructure ionic electronic film with a thickness of about 100 μm was prepared. The mold was then heated with a heat gun to release the film from the template and got sandwiched between graphene electrodes.

2.3. Multilayer Graphene Electrode Preparation. All the electrodes used in this study were covered on translucent PET substrates of a thickness of 25 μm. Graphene electrodes with different layers were grown on copper substrate by chemical vapor deposition (CVD), and then the grown graphene was transferred to PET substrate. A roll-to-roll process was used to realize volume production. Multilayer graphene films were accumulated by transferring single layers of graphene layer by layer (purchased from Ningbo soft carbon Electronic Science and Technology Co., Ltd.).

2.4. Characterization and Measurements. The surface morphology of the gel films was characterized by scanning electron microscopy (SEM, ZEISS Sigma 300). X-ray diffraction (XRD, Rigaku SmartLab SE XRD) was used to analyze the crystallinity of the gel film. The surface morphology and roughness of monolayer and bilayer graphene were observed by SEM and atomic force microscopy (AFM, NT-MDT TS-150, Moscow, Russia), respectively. An LCR instrument (IM3536, HIOKI) was used to measure the capacitance applied to an AC voltage of 125 mV at the frequency of 1 kHz. The external pressure loaded on our sensor was applied and recorded using a dynamometer with a computer-controlled workbench (Dongguan Zhiqu Precision Instrument Co., Ltd., 990-zq). A self-regulating acrylic sheet with the size of 1 cm × 1 cm was used as the pressure contact for the study. The capacitance–pressure response curves, response–hysteresis, and operational stability tests were all measured by utilizing the equipment. The response curve of the sensor is estimated by least square fitting.

2.5. Underwater Experimental Equipment. The pressure changes were realized by disturbing the water wave with a 250 mm diameter shafting propeller (Ningbo Qingfeng Model Co., Ltd.). The underwater static pressure at multi-depths induced variations of the output capacitance for real-time monitoring of the outputs in a special environment, which were recorded and stored by a microcontroller (STM32F103C8T6) linked to the sensor through the I/O interface. Data were sent through the serial port and dealt with using MATLAB 2017b software.

3. RESULTS AND DISCUSSION

3.1. Sensor Fabrication and TRM Characterization. A photograph of the final device is shown in Figure 1a. The IFS (1.5 cm × 2 cm) consists of five layers, and Ohmic contact is achieved by pasting 0.5 mm wide conductive copper tape on the edge of each electrode. The intermediate layer is the prepared TRM ionic gel electronic film, which is vertically sandwiched between two identical graphene electrodes. The
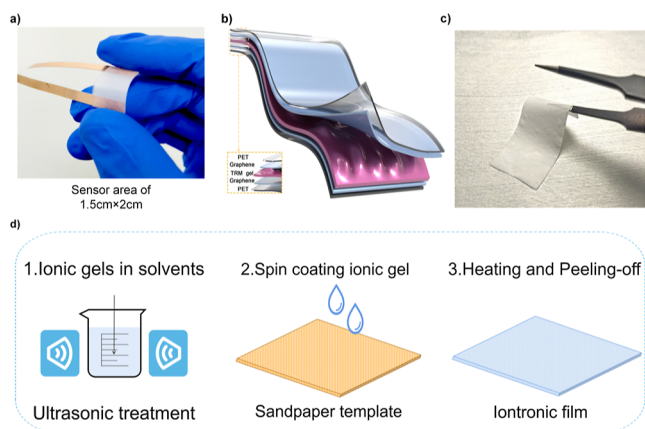

Figure 1. (a) Photograph of the final sensor. (b) Diagram of the sensor structure. The inset shows a cross-sectional view of the layers of PET/graphene/ionic gel film/Graphene/PET. (c) Photograph of the TRM ionic gel film. (d) Schematic of the fabrication sequence of ionic gel film.

above hierarchical structure overlaid on the PET substrate, as shown in the schematic of Figure 1b. The inset shows a cross-sectional view of different layers in the IFS. The graphene bottom electrode is in close contact with ionic gel electronic film, while an interface is formed between the top electrode and the rough surface of the film. In a sense, a layer with fixed electric charges of about ∼1 nm exists at the gel–electrode interface. The sensing mechanism of our fabricated sensor depends on the variations of contact area between the interface, which could lead to changes of the interface capacitance.[33,34] The structure of intermediate layer TRM is the key to area changes. As shown in Figure 1c, TRM film is a highly flexible and half-transparent independent ion electronic membrane. Figure 1d depicts the manufacturing sequence of TRM ionic gel electronic film. First, we prepared the premixed solution with ultrasound irradiation to stimulate multiple loose porous microstructures inside. The above operation is intended to form the exquisite first-scale microstructure of TRM. The porous-type gel formation mechanism can be explained by the synthesis of preordered aggregation of the molecular chain during the sonication. Second, the rough second-scale microstructure in TRM refers to the formation of larger uneven structures on the surface of ionic gels with a preset pattern as a template. Therefore, a solvent-free, independent solid, and retractable TRM electrolyte membrane was developed as a high capacitance dielectric material for flexible pressure sensors.

On the design of the rough second scale, sandpaper is an excellent preset template that plays a vital role in improving the shape coefficient (the ratio of compressed area to free expansion no-load surface area) and making the structure more accessible to deform during compression.[28] Generally, the smaller grit-no. sandpapers nos. 200 and 400 have higher roughness than less-indented surfaces nos. 600 and 1000, inducing relatively more straightforward changes in contact area during compression–release cycles and displaying more distinct capacitance variations. According to experimental verification produced by Yoon et al., the pressure sensor fabricated with a more significant characteristic size has higher sensitivity but reduces the linear range.[21] Still, we believe that high linearity is contributed to sensor calibrating and back-end circuit designing. This is why we choose sandpaper with grit-
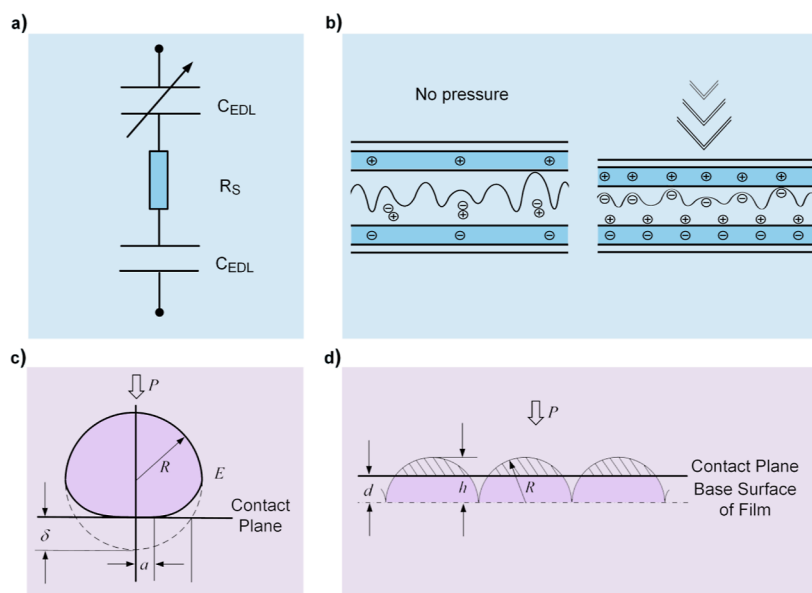
Figure 2. (a) Equivalent circuit for EDL. (b) Schematic of the formation mechanism of the EDL effect before and after applying pressure. (c) Schematic of unimodal elastic contact on the surface of the ionic gel film. (d) Contact schematic of the equivalent spherical rough surface of our ionic gel film.

no. 400 to make a compromise between sensitivity and linearity so as to meet the requirements of intended use. The random rugged microstructure on the surface of silicon carbide sandpapers with mesh numbers of 400 #, without any surfactant coating, is grafted onto the ionic gel electronic film in an efficient and economical way to form concave microstructures.

To further explore the structure and morphology characteristics of electrolyte films, XRD is used to analyze the effect of ultrasonic irradiation on the crystallinity with different concentrations, and the surface morphological features are examined using SEM. Figure S1a shows the XRD patterns of the unsonicated ionic gel films at different IL concentrations. As a comparative study, the films with different IL concentrations are fabricated by ultrasound treatment, as indicated in Table S1. The XRD patterns show that the peaks at a diffraction angle (2θ) of the unsonicated membranes are lower than that of ultrasound irradiation, which is more evident at high IL concentrations. The results can be explained by the high crystallinity and loose microstructure of P(VDF-HFP)/[EMIM][TFSI] ionic gel prepared by ultrasonic irradiation. Although the loose and porous microstructured films expand the linear working range, crystallinity has an essential influence on the ionic conductivity as well as sensitivity. In order to make up for these defects, the crystallinity can be decreased by adjusting the concentration of IL. Figure S1b shows the diffraction peaks of membranes having 30, 40, 60, and 80 wt % ILs, respectively. For membranes with 30 and 40 wt. % IL, the crystalline peaks are at the diffraction angles (2θ) of 12.5 and 20°. With the addition of [EMIM][TFSI] up to 60 and 80 wt %, the peak at $2\theta = 12.5°$ is no longer visible, and the relative intensity of the crystalline peak at $2\theta = 20°$ decreases, indicating an advance in the amorphicity of ionic gel. The peaks of the membranes with 60 and 80 wt.% of ILs do not change much under ultrasonic irradiation. Besides, the modulus of ionic gel becomes lower with high IL concentrations, and the liquid may be squeezed out under the high-pressure region, which will reduce the

sensitivity as the axial pressure loading.[35] For the sake of taking both mechanical properties and conductivity into account, this work selects 60 wt % concentration film with ultrasonic treatment as a research object. The quantitative information of film surface morphology from out of sandpaper template is studied by SEM at 2 and 20 μm, respectively. As shown in Figure S2, the surface of the cast formed ionic gel electronic film acquires microstructures opposite to the sandpaper template. The shape characteristics of these microstructures with a pore diameter of about 35 μm are irregular, and the concave positions are randomly distributed. At another scale, TRM membrane has a similar ellipsoidal structure, and films treated with ultrasound radiation reveal significantly more porosity composed of spheres with diameters of about 5 μm. It means that structurally, the gel films with TRM are expected to compensate for the stiffening effect with the increasing pressure and improve the overall linearity in the working range.

3.2. High Linearity Analysis. According to the classical Gouy−Chapman−Stern model, the EDL capacitance (C_{EDL}) can be divided into Helmholtz and diffuse layers that are simply modeled as two separate capacitive units C_H and C_D, respectively. The equivalent-circuit diagram may be regarded as a pair of EDL capacitances in series with an intermediate resistor (R_s), as shown in Figure 2a. Considering that both C_H and C_D are proportional to the change in contact area (A), C_{EDL} will be derived in the following format[20]

$$C_{EDL}^{-1} = \frac{1}{C_H} + \frac{1}{C_D} = UAC \times A \tag{1}$$

The great advantage in sensitivity of IFS stems from the extremely high unit area capacitance (UAC) caused by EDL effect. After a long period of research, UAC is mainly determined by the material properties of the electrode and the gel layer in relation to both the ionic species and concentration of ILs, the dielectric constant, and the thickness of the Helmholtz layer and also in connection with the surface potential of the electrode and the temperature of environments.[20] These material parameters remain constant during
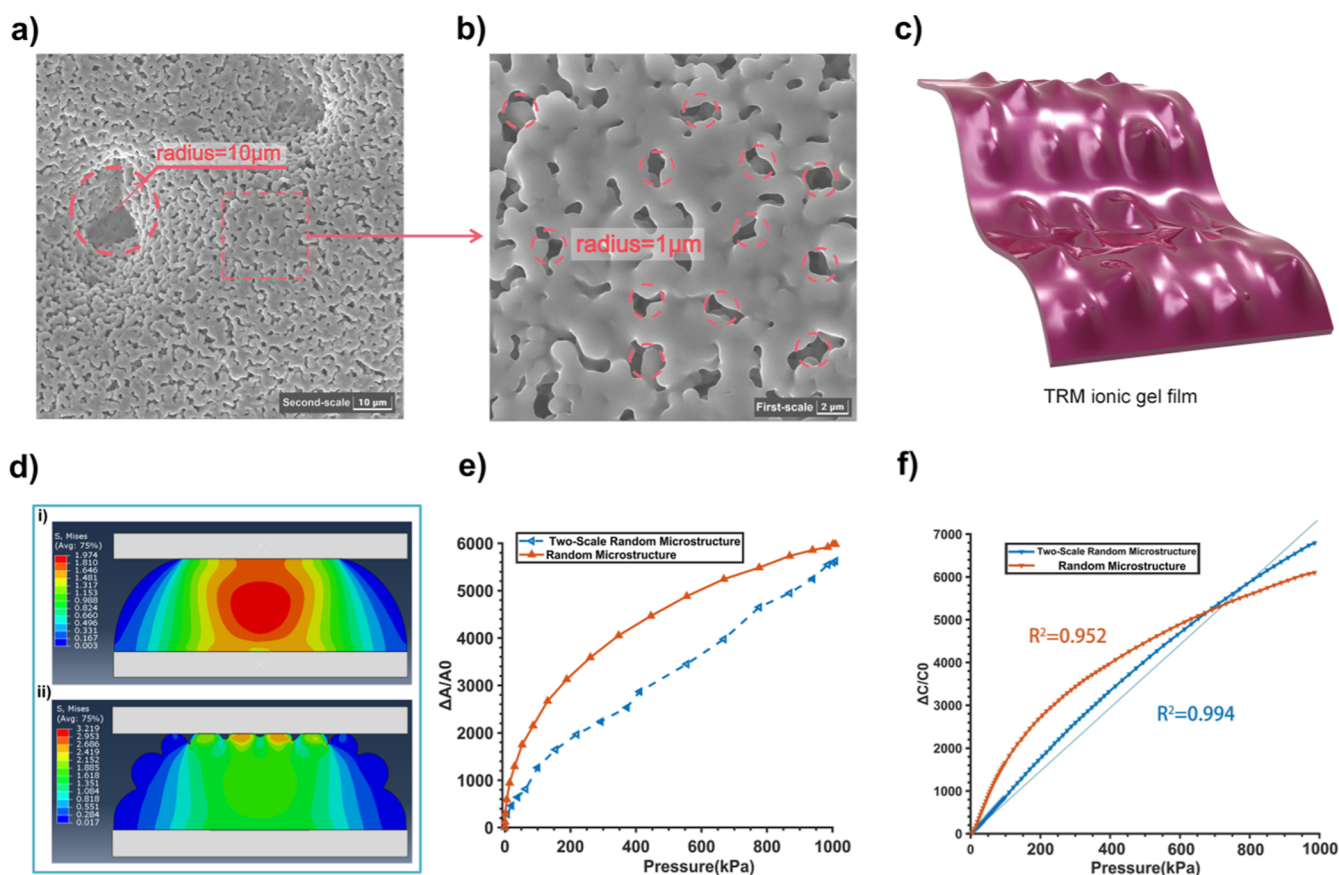
Figure 3. (a) SEM images of the second-scale microstructures with a scale bar of 10 μm. (b) SEM images of the first-scale micropores with a scale bar of 2 μm. (c) 3D schematic of TRM ionic gel film. (d) FEA of the deformation of ionic gel films with different microstructures upon compression: (i) injection-molded only second-scale microstructure ionic gel film using sandpaper as a template. (ii) TRM films after ultrasonic irradiation. (e) Contact area variation between the film with different microstructures and electrodes in a sensing range of 0−1 MPa. (f) Capacitance−pressure response curves of different microstructures at a pressure range up to 1 MPa.

the pressure response, so UAC can be regarded as a constant in a given system; thus, variations in the capacitance signal are only related to the change in the contact area. The aforementioned sensing process is schematically shown in Figure 2b.

Therefore, when the contact area is changed by applying pressure, the capacitance signal of the device is generated. The classical Persson theory in contact mechanics states that the actual contact is manifested in the deformation of surface roughness peaks when solid surfaces come into contact. The rugged peaks on film surfaces molded from sandpaper as templates (only the rough second scale) are usually simplified to oval hemispheres in shape.[28] Since the contact radius of an ellipsoid is much smaller than the size of electrolyte film, the rough peaks will be approximated as spheres. To be specific, the contact between the top electrode and electrolyte membrane can be reduced to a series of spheres deformed under pressure. In the light of elastic mechanical analysis, it is known that the contact area (A) of a single rough peak after deformation by normal direction pressure (P) satisfies the following equations[36]

$$\begin{cases} \delta = \left(\dfrac{9P^2}{16E^2R}\right)^{1/3} \\[2mm] a = \left(\dfrac{3PR}{4E}\right)^{1/3} \\[2mm] P = \dfrac{4}{3}ER^{1/2}\delta^{3/2} \\[2mm] A = \pi a^2 = \pi R\delta \end{cases} \tag{2}$$

where E is the modulus of elasticity, and δ, a, and R are the geometric parameters, which are shown in Figure 2c. For the whole rough surface, we simplified the model as the surface consists of n rough peaks with the same radius of curvature and height arranged on the ionic gel film, and these independent peaks are subjected to exactly the same load and deformation. As shown in Figure 2d, the maximum height of the rough peak above the base surface is h, and the normal direction deformation of the rough peak after compression is $h-d$. Assuming that each roughness peak is subjected to the same load P_i, the following equation can be derived from eq 3

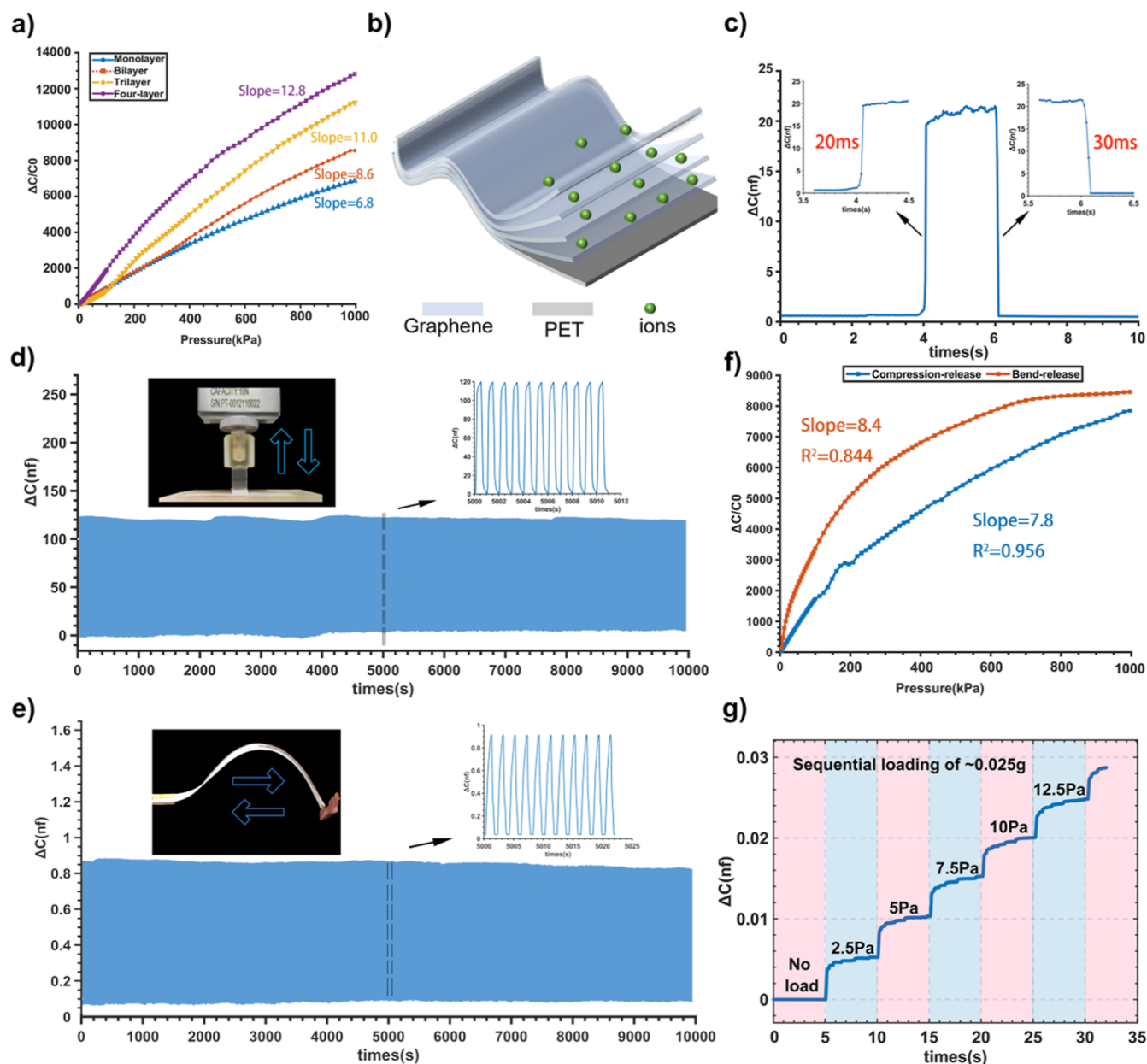$$P = nP_i = \frac{4}{3}nER^{1/2}(h - d)^{3/2} \tag{3}$$

Figure 4. Sensing performances of the TRM ionic gel and graphene-based electrode capacitive pressure sensor. (a) Capacitance–pressure response curves fabricated from graphene electrodes with different layers illustrating the sensitivities. (b) Schematic of diffusion and adsorption of ions between multilayer graphene. (c) Response and relaxation time of our sensor for a weight of 10 kPa pressure loading. (d) Compression–release mechanical stability under a loading pressure of 60 kPa for over 10,000 cycles. (e) Bend–release mechanical stability with a bending radius of curvature of 6 mm. (f) Capacitance–pressure response curves at a pressure range up to 1 MPa after 10,000 times compression–release test in (d) and 5000 times bend–release test in (e). (g) Illustration of LOD by sequential loading of the ultra-light 2.5 Pa objects.

The actual contact area between the electrode and ionic gel film is the sum of contact areas A_i of each roughness peak, which can be expressed as

$$A = nA_i = n\pi R(h - d) \tag{4}$$

Therefore, the relationship between contact area and normal direction pressure can be deduced as follows

$$P = \frac{4E}{3\pi^{3/2}n^{1/2}R^{1/2}}A^{3/2} \tag{5}$$

It can be seen that the normal direction pressure on the device is proportional to the 3/2 power of the contact area between the top electrode and gel, indicating that in terms of

the linear response, the films only with a second-scale microstructure have inherent defects. Specifically, the sensitivity of the entire response curve decreases with the increasing pressure, which is a common problem faced by iontronic pressure sensors.[28,37] During the compression of hemispherical bumps on the gel surface, the contact stress caused by unit displacement increases gradually. Due to the stiffening effect of gel films, the change rate of contact area decreases with the application of pressure, resulting in a nonlinear response of our device. To make up for the disadvantage, presonicating the mixed solution introduces small apertures on the surface of the second scale, which formed the first-scale microstructure. In TRM, second-scale

microstructures determine the linear interval and the deformation rate of the ionic membrane, while the first scale makes deformation more even and soft, which improves the linearity enormously in the entire working range. We studied the influence of the ratio of aperture size of two scales in TRM on linearity, as shown in Table S2. By increasing the frequency and time of ultrasonic processing, the linearity can be improved by increasing the aperture ratio gradually. However, too tiny apertures are not conducive to the improvement of linearity, and the overall linearity reaches the maximum at the aperture ratio of 10:1. The SEM images of the apertures in TRM are shown in Figure 3a,b.

By performing FEA, the high-linearity deformation mechanism can be in-depth elucidated. Compared to microstructures with only second-scale microstructures (just molded by sandpaper), the deflection in contact area with pressure is more linear in TRM films. For the oval-shaped TRM, Figure 3c illustrates the 3D schematic diagram of the thin electrolyte film structure with the rough surface. The distribution of normal direction pressure with the deformation of hemispherical bumps on the membrane is shown in Figure 3d (the more detailed dynamic information of ionic gel molded from sandpaper and TRM film is shown in Movies S1 and S2 of the Supporting Information, respectively). It could be considered that there is more uniform compression space in the case of TRM compared to only second-scale microstructures. As shown in curves of the normalized contact area shown in Figure 3e, the simulation indicates that the area deformation rate of TRM under specific pressure increases slowly, which represents that the change of membrane with TRM in the overall working range is relatively gentle. In general, the introduction of first-scale micropores builds a ladder structure on the hemisphere-shaped interface of rough second-scale microstructures. It brings more buffer space when the contact area of the interface varies during the compression. This step-by-step buffering shows a zigzag in the area variation curve obtained by FEA in Figure 3e, which, macroscopically, enables the stress deformation to be more uniform. Meanwhile, the high linearity of signals lies in the modulus matching between the ionic gel and electrodes with a flexible basement.[31] Ultrasonic treatment increases the Young's modulus of the ionic film, which puts the graphene electrodes and gel in a delicate equilibrium and finally achieves an increasement for linearity of the sensor. In order to further verify the linearity optimization effect of TRM, the capacitance−pressure response curves of electrolyte membranes with monolayer graphene electrode and different structures are shown in Figure 3f. The relative capacitance change curve of devices with only second-scale microstructures is similar to the results of other works using sandpaper-grafted microstructures,[32,38,39] and its linear range is not as good as that of our flexible iontronic sensor using TRM film (R^2 = 0.994). The response curve of the sensor is estimated by least square fitting. Particularly, it should be noted that the actual value of A_0 is smaller than the simulated results due to a few of the initial microstructures in contact with electrodes prior to pressurization.

3.3. Sensitivity Analysis and Other Sensing Properties. It is considered that sensitivity is one of the most crucial parameters,[17,20] which is defined by $S = \delta(\Delta C/C_0)/\delta P$, where C_0 and ΔC are the initial capacitance and the change in capacitance under the applied pressure (P), respectively. Notice that the graphene film with a large SSA can be utilized

as an excellent electrode. Compared with ITO substrate, the graphene-based device displays better sensitivity due to the higher UAC formed at the electrode−electrolyte interface.[18] Although the monolayer graphene electrode has shown higher interfacial capacitance than ITO,[40] the natural defects such as wrinkles and pores of graphene caused by growth and transfer are unfavorable for adsorption and diffusion of ions,[41] which restricts the UAC of graphene-based iontronic pressure devices. Multilayer graphene typically exhibits weak van der Waals interlayer interactions. By adjusting interlayer spacing, the multilayer graphene provides added active sites to absorb more ions and thus increase the interfacial capacitance. Therefore, we investigate the response curves of devices fabricated based on the roll-to-roll production of multilayer graphene with the same TRM films, as plotted in Figure 4a. The sensor with four-layer graphene electrodes has a pressure sensitivity of 12.8 kPa^{-1} under the whole working range, which is about twice as higher as that (6.8 kPa^{-1}) of monolayer graphene electrodes. It is worth noting that the linearity remains at $R^2 > 0.99$ after replacing electrodes with four-layer graphene, as shown in Figure S3. As summarized in Table S3, our TRM and multilayer graphene-based iontronic sensor shows an extraordinary linear response over a wide working range, not only enlarging the linear range but also presenting a good sensitivity. The sensitivity of devices is enhanced with the layer of graphene increasing, where the sensitivities of the bilayer and trilayer graphene devices are 8.6 and 11.0 kPa^{-1}, respectively. As mentioned above, multilayer graphene with sufficient interlayer spacing facilitates the entry of ions and induces more opposite charges in the electrode to increase the interfacial capacitance value.[42] The interlayer spacing facilitates the penetration of electrolyte ions from the broken edge of graphene and creates more active sites for reaction, as depicted in Figure 4b. In the embedding-based model, positive and negative ions in films, that is, $[EMIM]^+$ and $[TFSI]^-$, are assumed as equivalent spheres with van der Waals radii of 0.281 and 0.326 nm, respectively.[43] Therefore, the interlayer spacing of multilayer graphene should be large enough to accommodate ion insertion. The few-layer graphene transferred to PET substrate by the roll-to-roll process is suitable for large-area electrode production. The natural morphology of CVD produced multilayer graphene contains parts of amorphous carbon, which manifests as white carbon spheres in the SEM images of Figure S4a. AFM images of Figure S4b reveal that the presence of embedded carbon spheres and their surrounding folds are about tens of nanometers in thickness, which act as scaffolds to expand interlayer spacing. It has been proven that the measure effectively avoids the self-restacking of graphene nanosheets and thereby improve the ion-accessible surface area.[44] What in fact is measured is a height profile of a fold created by the particle that is stuck, perhaps, between or underneath the layers. Therefore, the multilayer graphene film with a significant volume of amorphous carbon scaffolds naturally improves the transmission efficiency of electrolyte ions and achieves an ultra-high interface capacitance. In general, the increase in capacitance brings a leap in sensitivity.

Furthermore, the other critical parameters of our sensor with TRM ionic gel film and four-layer graphene electrodes have been investigated. To test the response and relaxation speed of the device, a weight of 10 kPa pressure was applied on the sensor. As shown in Figure 4c, the capacitance fluctuated abruptly with the pressure placed on our sensor loading and uploading, which is followed by obvious changes showing the
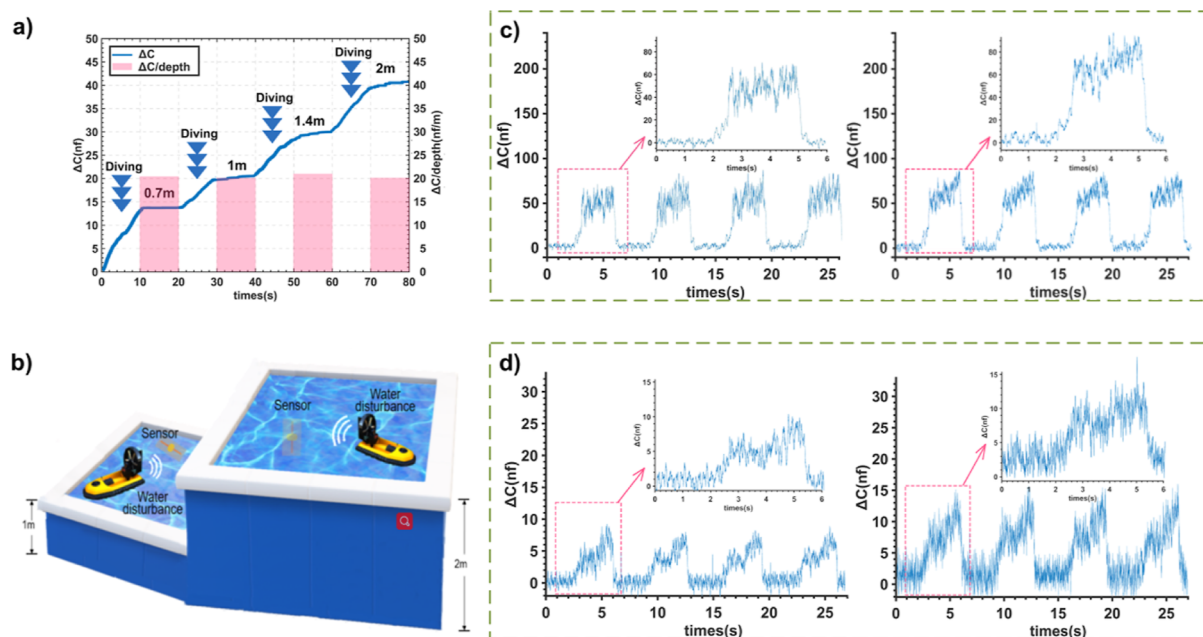
Figure 5. Underwater experiments of the iontronic pressure sensor. (a) Capacitance corresponding to the increased depth in the water tank. (b) Schematic demonstration of the water disturbance detection of the sensor. Adjusting the speed of the propeller at 50 (left figure) and 100 rad/s (right figure), the time domain water disturbance is detected using our sensor at water depths of 1 m (c) and 2 m (d), respectively. The inset shows the waveform of a single periodic wave envelope.

response and relaxation times are 20 and 30 ms, respectively. Undergo compression and recovery, the TRM films contain a lot of voids and air gaps, leaving ample spacing to store and release energy to reduce the viscoelasticity of electrode—electrolyte. The mechanical stability of the sensor is a demanded property that determines the reliability over long-term operation. The sensor exhibits excellent performance and stable response over compression—release under a loading pressure of 60 kPa for over 10,000 cycles, showing low signal drift (Figure 4d). The outstanding mechanical stability results from the abundant porous structure of TRM films and the excellent fracture strength of graphene electrodes. It is worth mentioning that the low signal drift occurs in about 100 cycles, which is caused by the plastic deformation of the TRM porous structure under repeated stress. After the pressure is removed, the loose TRM with spring-back properties recovers to the initial state, while the stable C—C bond between graphene layers ensures that the electrode remains stable after repeated compressions. Figure 4e reveals that the sensor shows basically unchanged over 5000 bend—release cycles with a bending radius of curvature of 6 mm. In this way, our sensor with conformal attachment capability is expected to be attached to the surface of soft robots for monitoring the external environment and motion status. However, as shown in Figure 4f, the sensitivity and linearity of sensors have slight decreases after 5000 bend—release cycles under the entire working range, and the response curve fluctuates slightly after multiple compressions and releases. In addition, the ultra-lightweight object detection response determines the pressure resolution of our sensor. We sequentially loaded the slight pressure on the surface of the sensor, which exhibits a low LOD of 25 mg (~2.5 pa), as shown in Figure 4g.

3.4. Application of the Sensor for Water Wave Detection at Different Depths. Sensors with high linearity over the entire operating range can collect the changes of capacitance in a large pressure-difference environment without

using additional signal processing modules. Thus, we designed an experiment to confirm the superior performance of our sensor in the underwater environment. It can be proved that the sensor maintains a highly linear response by dropping the sensor into a pool to detect underwater static pressure at different depths. Our sensor was connected with a microcontroller through the I/O interface; recording and storing variations in capacitance were caused by static pressure to form a pressure monitoring system. As we gradually sank the monitoring system into a water tank (Fig. S5) and left it at 0.7, 1, 1.4, and 2 m in sequence from the water surface for 10 s, the capacitance as a function of time was recorded. With increasing water depth, the system exhibits a stepped capacitance increase that is proportional to the added static pressure at a rate of about 20 nF/m (Figure 5a). The experiment shows that the monitoring system has extraordinary potential to sense the underwater static pressure change due to its high linearity.

The outstanding linearity permits the sensor to monitor vibrational stimuli at different water depths. Here, we exhibit the performance of the sensor to measure water wave disturbance signals; the specific scene is shown in Figure 5b. We used an adjustable speed propeller to simulate the pressure disturbance of water flow caused by stern. Let the speed of the propeller work at 50 and 100 rad/s, respectively. The pressure monitoring system was attached to the pool wall with water depths of 1 and 2 m to detect the dynamic pressure caused by water disturbance. Figure 5c illustrates the changes of pressure measured at different rotational speeds at a depth of 1 m. Several groups of capacitive signal waveforms were detected with approximate amplitudes, and the oscillation amplitude of the capacitance value decay as the propeller speed decreases. After moving the monitoring system to a water depth of 2 m, the vibration intensity of capacitance was weakened due to the dissipation of wave disturbance intensity as the water depth increased (Figure 5d). The gentler flow disturbance is represented by greater noise in the capacitance signal, while

the high sensitivity of our sensor ensures that the basic waveform is not lost. In addition to its excellent sensitivity, the excellent LOD allows the TRM sensor to sense the ripples generated by distant weak vortex. The sensor was attached to the water surface of the side wall of the aquarium, and the propeller speed was adjusted to the minimum (3 rad/s) and placed 50 cm away to generate a weak vortex, as shown in Figure S6. The capacitance value changes of the sensor during the process from the propeller stop to startup are shown in Figure S7, and the slight pressure disturbance caused by the ripples is clearly reflected in the sensor. The mentioned experiment indicates that our sensor is expected to be attached to underwater software robots to detect the water wave pressure disturbances induced by ships or submersibles.[45−47]

4. CONCLUSIONS

In summary, we have designed and fabricated high-linearity (over the entire working range) IFSs that benefit from the TRM gel. The FEA simulation and experimental results indicate that the TRM enables a smoother contact area change between electrolyte film and electrodes under pressure. Furthermore, due to the embedded carbon spheres and their surrounding folds enhancing the interlayer spacing and ion-accessible surface area, multilayer graphene electrodes effectively promote the migration and diffusion of ions and thereby improve the device sensitivity. This work provides an optimized approach on the design of microstructured ionic gel and active electrode material, which not only enlarges the linear range but also presents a good sensitivity. The extraordinary linear response over a wide working range is beneficial to our sensor to work in the underwater environment with significant pressure differences. This work opens a door for static pressure detection at different water depths and dynamic pressure mapping caused by the propeller.

ASSOCIATED CONTENT

Ⓢ Supporting Information

The Supporting Information is available free of charge at https://pubs.acs.org/doi/10.1021/acsomega.2c05186.

> FEA simulation of the film only with second-scale microstructures and TRM (MOV)
> FEA simulation of the TRM film (MOV)
> Material ratio and process parameters used in preparation of ionic film; experiment data of aperture size on linearity; comparison of the performance of our work with existing capacitive sensors; XRD patterns of the film only with second-scale microstructure and TRM; SEM images of the film only with second-scale microstructure and TRM; response curves of sensors fabricated from graphene electrodes with different layers; SEM images of monolayer graphene and bilayer graphene on translucent PET substrates; contact-mode AFM image of the monolayer and bilayer graphene films transferred on a PET film; and photos, schematics, and results of innovative application (PDF)

AUTHOR INFORMATION

Corresponding Author

Jiafei Hu − *College of Intelligent Science, National University of Defense Technology, Changsha 410073, China;* ⓞ orcid.org/0000-0001-9146-0982; Email: hjf_sensor@163.com

Authors

Shaowei Wu − *College of Intelligent Science, National University of Defense Technology, Changsha 410073, China;* ⓞ orcid.org/0000-0003-3152-8943

Chengxiu Yang − *College of Intelligent Science, National University of Defense Technology, Changsha 410073, China;* ⓞ orcid.org/0000-0003-4734-7995

Mengchun Pan − *College of Intelligent Science, National University of Defense Technology, Changsha 410073, China*

Weicheng Qiu − *College of Intelligent Science, National University of Defense Technology, Changsha 410073, China*

Yanrui Guo − *College of Intelligent Science, National University of Defense Technology, Changsha 410073, China*

Kun Sun − *College of Intelligent Science, National University of Defense Technology, Changsha 410073, China*

Yujing Xu − *College of Intelligent Science, National University of Defense Technology, Changsha 410073, China*

Peisen Li − *College of Intelligent Science, National University of Defense Technology, Changsha 410073, China*

Junping Peng − *College of Intelligent Science, National University of Defense Technology, Changsha 410073, China*

Qi Zhang − *College of Intelligent Science, National University of Defense Technology, Changsha 410073, China*

Complete contact information is available at:
https://pubs.acs.org/10.1021/acsomega.2c05186

Author Contributions

All authors commented on the manuscript and checked the results. S.W. conceived the idea, fabricated and characterized the device, prepared the figures, and wrote the manuscript. Y.C. assisted in completing the experiment and modified the manuscript many times. Y.X. and W.Q. assisted in the finite element simulation and reviewed the results. P.L. and K.S. assisted in the preparation and processing of the device. J.P. and Y.G. assisted with the device characterization and measurements. J.H., Q.Z., and M.P. provided regular guidance to the research and revised the manuscript.

Notes

The authors declare no competing financial interest.

REFERENCES

(1) Zhang, S.; Zhu, J.; Zhang, Y.; Chen, Z.; Song, C.; Li, J.; Yi, H.; Qiu, D.; Guo, K.; Zhang, C.; Pan, T.; Lin, Y.; Zhou, H.; Long, H.; Yang, H.; Cheng, H. Standalone stretchable RF systems based on asymmetric 3D microstrip antennas with on-body wireless communication and energy harvesting. *Nano Energy* **2022**, *96*, 107069.

(2) Yi, N.; Gao, Y.; Verso, A. L., Jr.; Zhu, J.; Erdely, D.; Xue, C.; Lavelle, H.; Cheng, H. Fabricating functional circuits on 3D freeform surfaces via intense pulsed light-induced zinc mass transfer. *Mater. Today* **2021**, *50*, 24−34.

(3) Qu, X.; Liu, Z.; Tan, P.; Wang, C.; Liu, Y.; Feng, H.; Luo, Z. L.; Li, Z.; Wang, Z. L. Artificial tactile perception smart finger for material identification based on triboelectric sensing. *Sci. Adv.* **2022**, *8*, No. eabq2521.

(4) An, X.; Wang, C.; Shao, R.; Sun, S. Advances and prospects of triboelectric nanogenerator for self-powered system. *Int. J. Smart Nano Mater.* **2021**, *12*, 233−255.

(5) Jia, Y.; Jiang, Q.; Sun, H.; Liu, P.; Hu, D.; Pei, Y.; Liu, Y.; Crispin, X.; Fabiano, S.; Ma, Y.; Cao, Y. Wearable Thermoelectric Materials and Devices for Self-Powered Electronic Systems. *Adv. Mater.* **2021**, *33*, 2102990.

(6) Ruth, S. R. A.; Feig, V. R.; Tran, H.; Bao, Z. Microengineering Pressure Sensor Active Layers for Improved Performance. *Adv. Funct. Mater.* **2020**, *30*, 2003491.

(7) Hammock, M. L.; Chortos, A.; Tee, C. K.; Tok, B. H.; Bao, Z. 25th anniversary article: The evolution of electronic skin (e-skin): a brief history, design considerations, and recent progress. *Adv. Mater.* **2013**, *25*, 5997.

(8) Mishra, R. B.; El-Atab, N.; Hussain, A. M.; Hussain, M. M. Recent Progress on Flexible Capacitive Pressure Sensors: From Design and Materials to Applications. *Adv. Mater. Technol.* **2021**, *6*, 2001023.

(9) Chen, X.; Li, R.; Niu, G.; Xin, M.; Xu, G.; Cheng, H.; Yang, L. Porous graphene foam composite-based dual-mode sensors for underwater temperature and subtle motion detection. *Chem. Eng. J.* **2022**, *444*, 136631.

(10) Huang, Y.; Fan, X.; Chen, S. C.; Zhao, N. Emerging Technologies of Flexible Pressure Sensors: Materials, Modeling, Devices, and Manufacturing. *Adv. Funct. Mater.* **2019**, *29*, 1808509.

(11) Zhan, Z.; Lin, R.; Tran, V. T.; An, J.; Wei, Y.; Du, H.; Tran, T.; Lu, W. A Paper-Carbon Nanotube Based Wearable Pressure Sensor for Physiological Signal Acquisition and Soft Robotic Skin. *ACS Appl. Mater. Interfaces* **2017**, *9*, 37921.

(12) Lou, Z.; Chen, S.; Wang, L.; Jiang, K.; Shen, G. An ultra-sensitive and rapid response speed graphene pressure sensors for electronic skin and health monitoring. *Nano Energy* **2016**, *23*, 7−14.

(13) Zhu, Z.; Li, R.; Pan, T. Imperceptible Epidermal−Iontronic Interface for Wearable Sensing. *Adv. Mater.* **2018**, *30*, 1705122.

(14) Eom, J.; Heo, J. S.; Kim, M.; Lee, J. H.; Park, S. K.; Kim, Y. H. Highly sensitive textile-based strain sensors using poly(3,4-ethyl-enedioxythiophene):polystyrene sulfonate/silver nanowire-coated nylon threads with poly-L-lysine surface modification. *RSC Adv.* **2017**, *7*, 53373−53378.

(15) Keum, K.; Eom, J.; Lee, J. H.; Heo, J. S.; Park, Y. H.; Kim, Y.-H. Fully-integrated wearable pressure sensor array enabled by highly sensitive textile-based capacitive ionotronic devices. *Nano Energy* **2021**, *79*, 105479.

(16) Ntagios, M.; Nassar, H.; Pullanchiyodan, A.; Navaraj, W. T.; Dahiya, R. Robotic Hands with Intrinsic Tactile Sensing via 3D Printed Soft Pressure Sensors. *Adv. Intell. Syst.* **2020**, *2*, 1900080.

(17) He, Y.; Wu, J.; Lin, M.; Xiao, S.; Liu, H.; Zhou, P. Ionic flexible force sensors and their potential applications. *J. Mater. Chem. C* **2021**, *9*, 16378.

(18) Wang, H.; Li, Z.; Liu, Z.; Fu, J.; Shan, T.; Yang, X.; Lei, Q.; Yang, Y.; Li, D. Flexible capacitive pressure sensors for wearable electronics. *J. Mater. Chem. C* **2022**, *10*, 1594.

(19) Tang, Z.; Scriven, L. E.; Davis, H. T. A three-component model of the electrical double layer. *J. Chem. Phys.* **1992**, *97*, 494−503.

(20) Chang, Y.; Wang, L.; Li, R.; Zhang, Z.; Wang, Q.; Yang, J.; Guo, C. F.; Pan, T. First decade of interfacial iontronic sensing: from droplet sensors to artificial skins. *Adv. Mater.* **2021**, *33*, 2003464.

(21) Yoon, S. G.; Park, B. J.; Chan, S. T. Highly Sensitive Piezocapacitive Sensor for Detecting Static and Dynamic Pressure Using Ion-Gel Thin Films and Conductive Elastomeric Composites. *ACS Appl. Mater. Interfaces* **2017**, *9*, 36206.

(22) Ren, Y.; Liu, Z.; Jin, G.; Yang, M.; Shao, Y.; Li, W.; Wu, Y.; Liu, L.; Yan, F. Electric-Field-Induced Gradient Ionogels for Highly Sensitive, Broad-Range-Response, and Freeze/Heat-Resistant Ionic Fingers. *Adv. Mater.* **2021**, *33*, 2008486.

(23) Wang, H.; Wang, Z.; Yang, J.; Xu, C.; Zhang, Q.; Peng, Z. Ionic Gels and Their Applications in Stretchable Electronics. *Macromol. Rapid Commun.* **2018**, *39*, 1800246.

(24) Yang, J. C.; Kim, J. O.; Oh, J.; Kwon, S. Y.; Kim, D. W. Microstructured Porous Pyramid-based Ultra-high Sensitive Pressure Sensor Insensitive to Strain and Temperature. *ACS Appl. Mater. Interfaces* **2019**, *11*, 19472.

(25) Xue, N.; Gao, G.; Sun, J.; Liu, C.; Li, T.; Chi, C. SystematicStudy and Experiment of a Flexible Pressure and Tactile SensingArray for Wearable Devices Applications. *J. Micromech. Microeng.* **2018**, *28*, 075019.

(26) Boutry, C.; Negre, M.; Jorda, M.; Vardoulis, O.; Chortos, Z.; Khatib, O.; Bao, Z. A hierarchically patterned, bioinspired e-skin able to detect the direction of applied pressure for robotics. *Sci. Robot.* **2018**, *3*, No. eaau6914.

(27) Luo, Y.; Shao, Y.; Chen, S.; Hongmiao, X.; Xiangming, T. Flexible Capacitive Pressure Sensor Enhanced by Tilted Micropillar Arrays. *ACS Appl. Mater. Interfaces* **2019**, *11*, 17796.

(28) Chhetry, A.; Kim, J.; Yoon, H.; Park, J. Y. An Ultrasensitive Interfacial Capacitive Pressure sensor based on a Randomly Distributed Microstructured Iontronic Film for Wearable Applications. *ACS Appl. Mater. Interfaces* **2019**, *11*, 3438.

(29) Bai, N.; Wang, L.; Wang, Q.; Deng, J.; Wang, Y.; Lu, P.; Huang, J.; Li, G.; Zhang, Y.; Yang, J. Graded intrafillable architecture-based iontronic pressure sensor with ultra-broad-range high sensitivity. *Nat. Commun.* **2020**, *11*, 209.

(30) Qiu, Z.; Wan, Y.; Zhou, W.; Yang, J.; Yang, J.; Huang, J.; Zhang, J.; Liu, Q.; Huang, S.; Bai, N.; Wu, Z.; Hong, W.; Wang, H.; Guo, C. F. Ionic skin with biomimetic dielectric layer templated from calathea zebrine leaf. *Adv. Funct. Mater.* **2018**, *28*, 1802343.

(31) Lu, P.; Wang, L.; Zhu, P.; Huang, J.; Guo, C. F. Iontronic pressure sensor with high sensitivity and linear response over a wide pressure range based on soft micropillared electrodes. *Sci. Bull.* **2021**, *66*, 1091.

(32) Xiao, Y.; Duan, Y.; Li, N.; Wu, L.; Meng, B.; Tan, F.; Lou, Y.; Wang, H.; Zhang, W.; Peng, Z. Multilayer Double-Sided Micro-structured Flexible Iontronic Pressure Sensor with a Record-wide Linear Working Range. *ACS Sens.* **2021**, *6*, 1785−1795.

(33) Yang, J.; Liu, Q.; Deng, Z.; Gong, M.; Lei, F.; Zhang, J.; Zhang, X.; Wang, Q.; Liu, Y.; Wu, Z.; Guo, C. F. Ionic liquid−activated wearable electronics. *Mater. Today Phys.* **2019**, *8*, 78−85.

(34) Yuan, C.; et al. Preparation and characterization of a novel ionic conducting foam-type polymeric gel based on polymer PVdF-HFP and ionic liquid [EMIM][TFSI]. *Colloid Polym. Sci.* **2015**, *293*, 1945−1952.

(35) Li, S.; Pan, N.; Zhu, Z.; Li, R.; Li, B.; Chu, J.; Li, G.; Chang, Y.; Pan, T. All-in-One Iontronic Sensing Paper. *Adv. Funct. Mater.* **2019**, *29*, 1807343.

(36) Wen, S.; Huang, P.*Principles of Tribology*; Tsinghua University Press: Beijing, China, 2012; pp 219−220.

(37) Liu, Q.; Liu, Y.; Shi, J.; Liu, Z.; Wang, Q.; Guo, C. F. High-Porosity Foam-Based Iontronic Pressure Sensor with Superhigh Sensitivity of 9280 kPa− 1. *Nano-Micro Lett.* **2022**, *14*, 1−12.

(38) Wang, P.; Li, G.; Yu, W.; Meng, C.; Guo, S. Flexible Pseudocapacitive Iontronic Tactile Sensor Based on Microsphere-Decorated Electrode and Microporous Polymer Electrolyte for Ultrasensitive Pressure Detection. *Adv. Electron. Mater.* **2022**, *8*, 2101269.

(39) Cai, M. X.; Yang, Y. J.A Wireless Cardiovascular Pressure Sensor Based on an Iontronic Film with High Sensitivity. In *2021 IEEE 34th International Conference on Micro Electro Mechanical Systems (MEMS)*; IEEE, 2021.

(40) Nie, B.; Li, R.; Cao, J.; Brandt, J. D.; Pan, T. Flexible Transparent Iontronic Film for Interfacial Capacitive Pressure Sensing. *Adv. Mater.* **2015**, *27*, 6055.

(41) Xue, Y.; Zhang, Q.; Wang, W.; Cao, H.; Yang, Q.; Fu, L. Opening Two-Dimensional Materials for Energy Conversion and Storage: A Concept. *Adv. Energy Mater.* **2017**, *7*, 1602684.

(42) Li, Z.; Gadipelli, S.; Li, H.; Howard, C. A.; Dan, J.; Shearing, P. R.; Guo, Z.; Parkin, I. P.; Li, F. Tuning the interlayer spacing of graphene laminate films for efficient pore utilization towards compact capacitive energy storage. *Nat. Energy* **2020**, *5*, 160.

(43) Beichel, W.; Eiden, P.; Krossing, I. Establishing consistent van der Waals volumes of polyatomic ions from crystal structures. *ChemPhysChem* **2013**, *14*, 3221−3226.

(44) Wu, S.; Hui, K.; Hui, K. N.; Yun, J. M.; Kim, K. H. A novel approach to fabricate carbon sphere intercalated holey graphene electrode for high energy density electrochemical capacitors. *Chem. Eng. J.* **2017**, *317*, 461−470.

(45) Gao, L.; Wang, M.; Wang, W.; Xu, H.; Wang, Y.; Zhao, H.; Li, L. Highly sensitive pseudocapacitive iontronic pressure sensor with broad sensing range. *Nano-Micro Lett.* **2021**, *13*, 140.

(46) Niu, H.; Li, H.; Gao, S.; Li, Y.; Wei, X.; Chen, Y.; Yue, G.; Zhou, W.; Shen, G. Perception-to-Cognition Tactile Sensing Based on Artificial-Intelligence-Motivated Human Full-Skin Bionic Electronic Skin. *Adv. Mater.* **2022**, *34*, 2202622.

(47) Yang, M.; Cheng, Y.; Yue, Y.; Chen, Y.; Gao, H.; Li, L.; Gao, Y. High-Performance Flexible Pressure Sensor with a Self-Healing Function for Tactile Feedback. *Adv. Sci.* **2022**, *9*, 2200507.